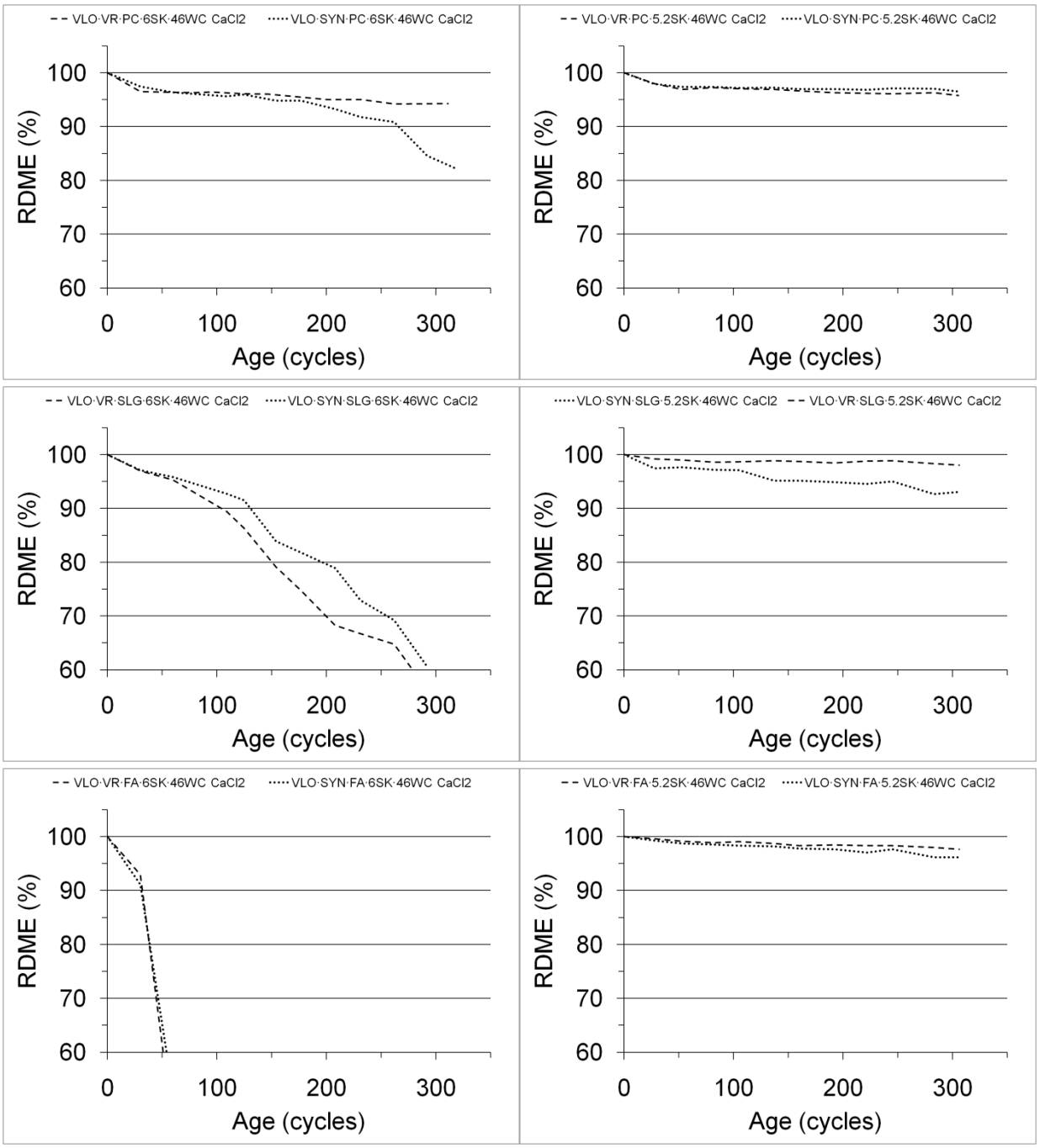

Figure 36: Relative dynamic modulus of elasticity plots for the Phase III very low air content 0.46 *w/cm* mixtures frozen in a 4.0 wt. % $CaCl_2$ brine. From left to right, 564 lbs/yd^3 CMC mixtures vs. 490 lbs/yd^3 CMC mixtures. From top to bottom: straight portland cement mixtures, 40 wt. % substitution slag cement mixtures, and 25 wt. % substitution fly ash mixtures. Dashed lines denote mixtures with vinsol resin AEA; dotted lines denote mixtures with synthetic AEA.

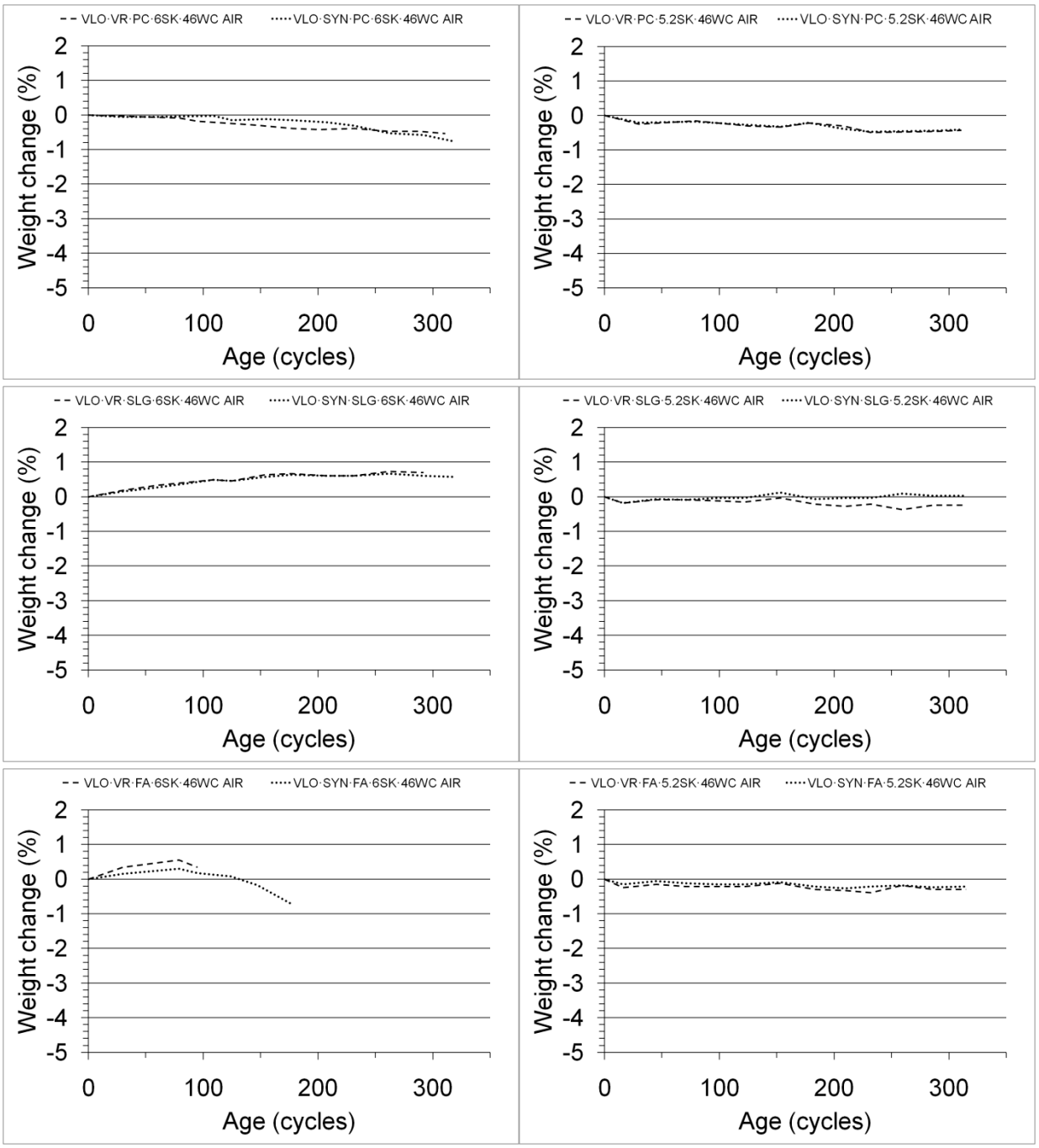

Figure 37: Weight change plots for the Phase III very low air content 0.46 *w/cm* mixtures frozen in air (ASTM C666 Procedure B). From left to right, 564 lbs/yd^3 CMC mixtures vs. 490 lbs/yd^3 CMC mixtures. From top to bottom: straight portland cement mixtures, 40 wt. % substitution slag cement mixtures, and 25 wt. % substitution fly ash mixtures. Dashed lines denote mixtures with vinsol resin AEA; dotted lines denote mixtures with synthetic AEA.

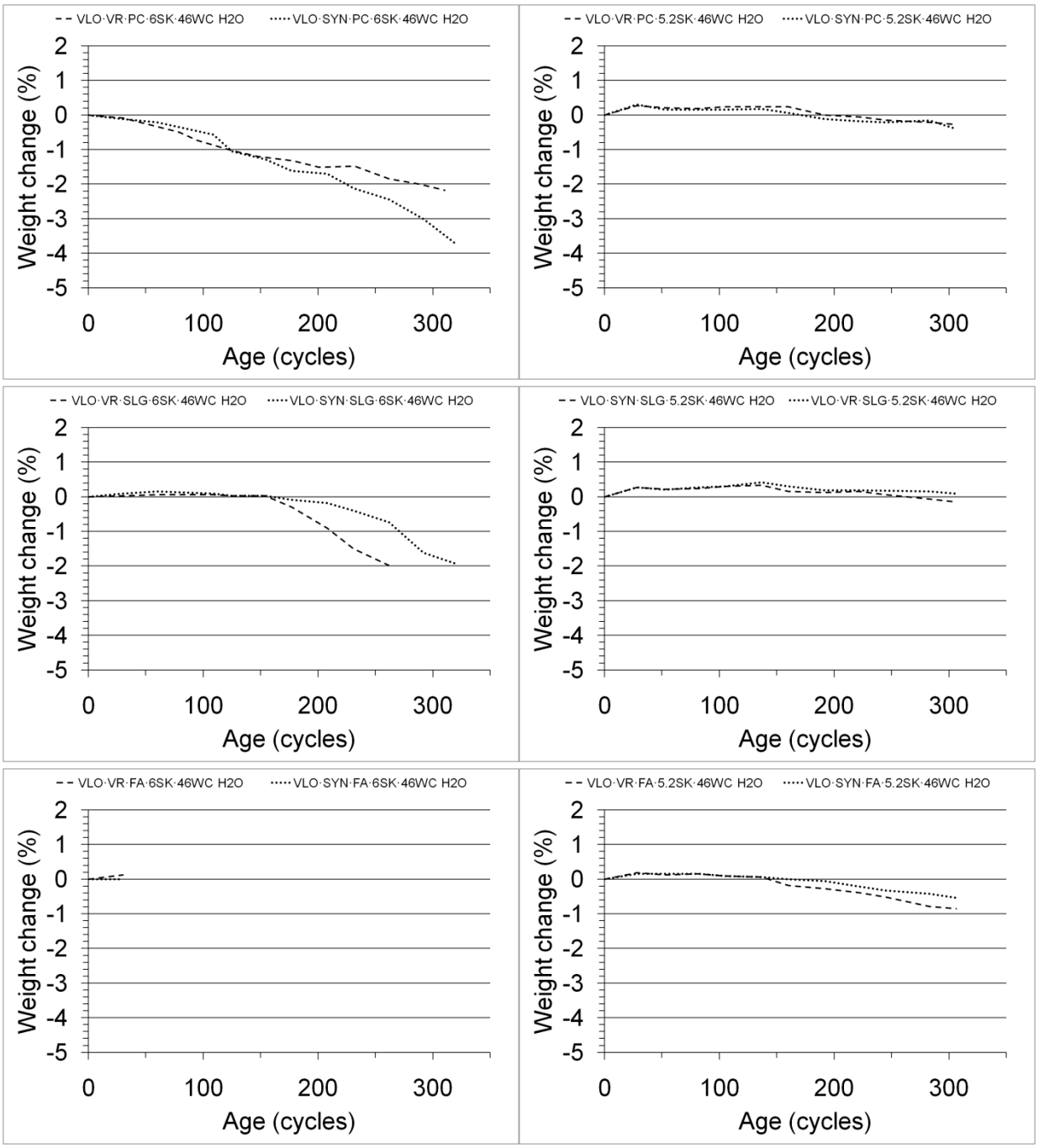

Figure 38: Weight change plots for the Phase III very low air content 0.46 *w/cm* mixtures frozen in water (ASTM C666 Procedure A). From left to right, 564 lbs/yd^3 CMC mixtures vs. 490 lbs/yd^3 CMC mixtures. From top to bottom: straight portland cement mixtures, 40 wt. % substitution slag cement mixtures, and 25 wt. % substitution fly ash mixtures. Dashed lines denote mixtures with vinsol resin AEA; dotted lines denote mixtures with synthetic AEA.

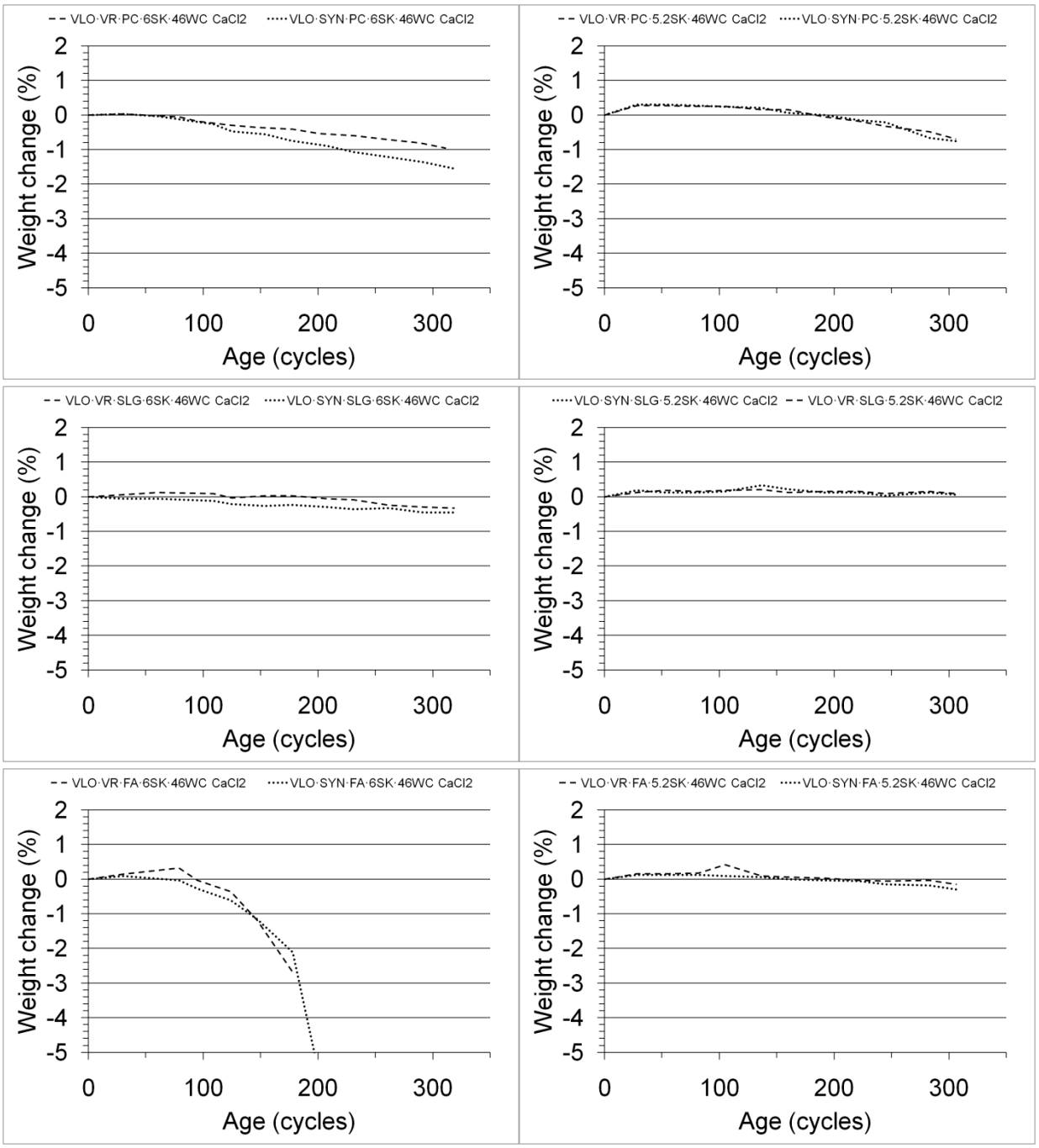

Figure 39: Weight change plots for the Phase III very low air content 0.46 *w/cm* mixtures frozen in a 4.0 wt. % $CaCl_2$ brine. From left to right, 564 lbs/yd^3 CMC mixtures vs. 490 lbs/yd^3 CMC mixtures. From top to bottom: straight portland cement mixtures, 40 wt. % substitution slag cement mixtures, and 25 wt. % substitution fly ash mixtures. Dashed lines denote mixtures with vinsol resin AEA; dotted lines denote mixtures with synthetic AEA.

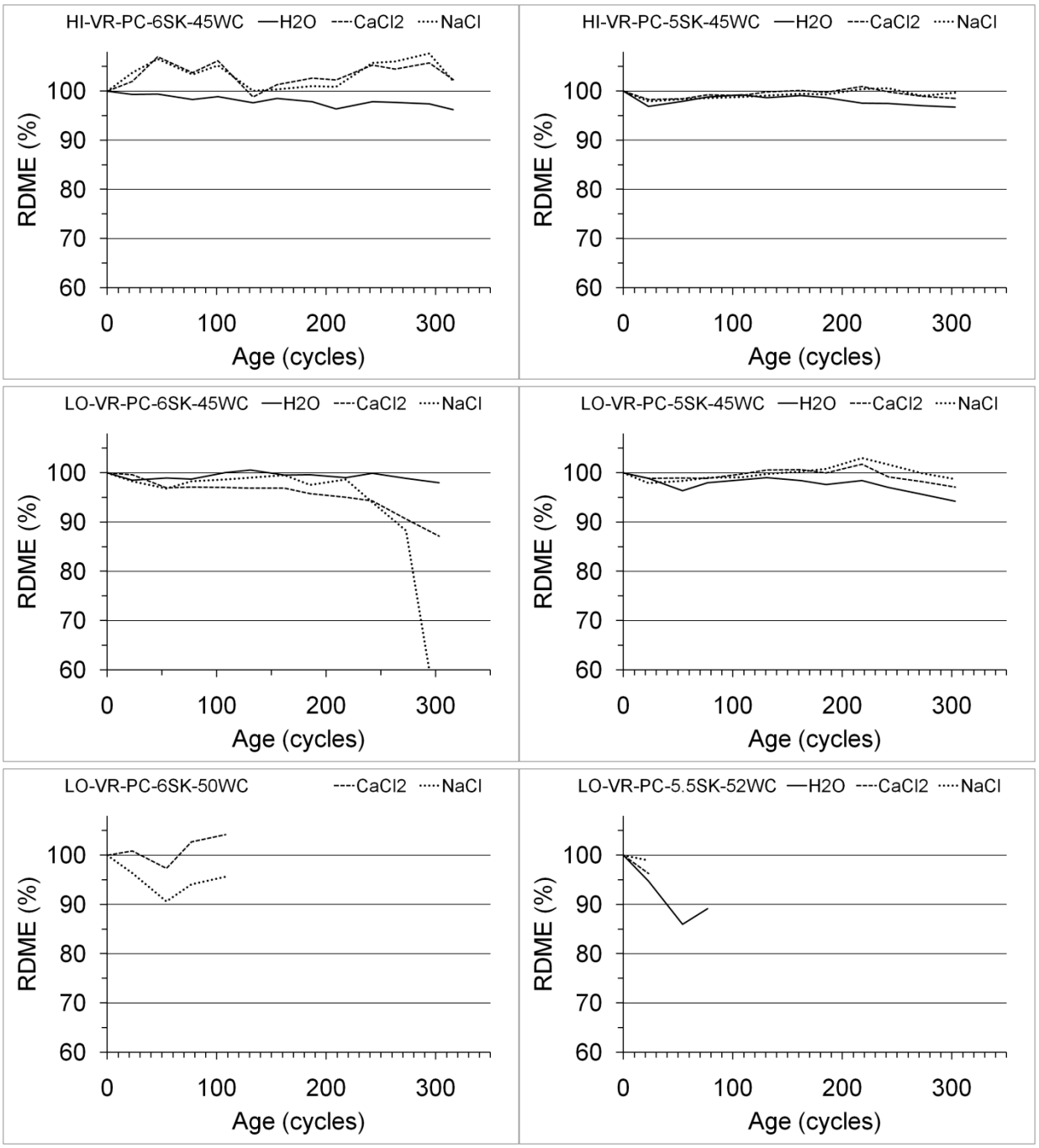

Figure 40: Relative dynamic modulus of elasticity plots from selected Phase II concrete mixtures exposed to extended F-T cycling test results under different ASTM C66 Procedure A freezing regimes: freeze in water, freeze in 4.0 wt % $CaCl_2$ brine, and freeze in 4.2 wt. % NaCl brine.

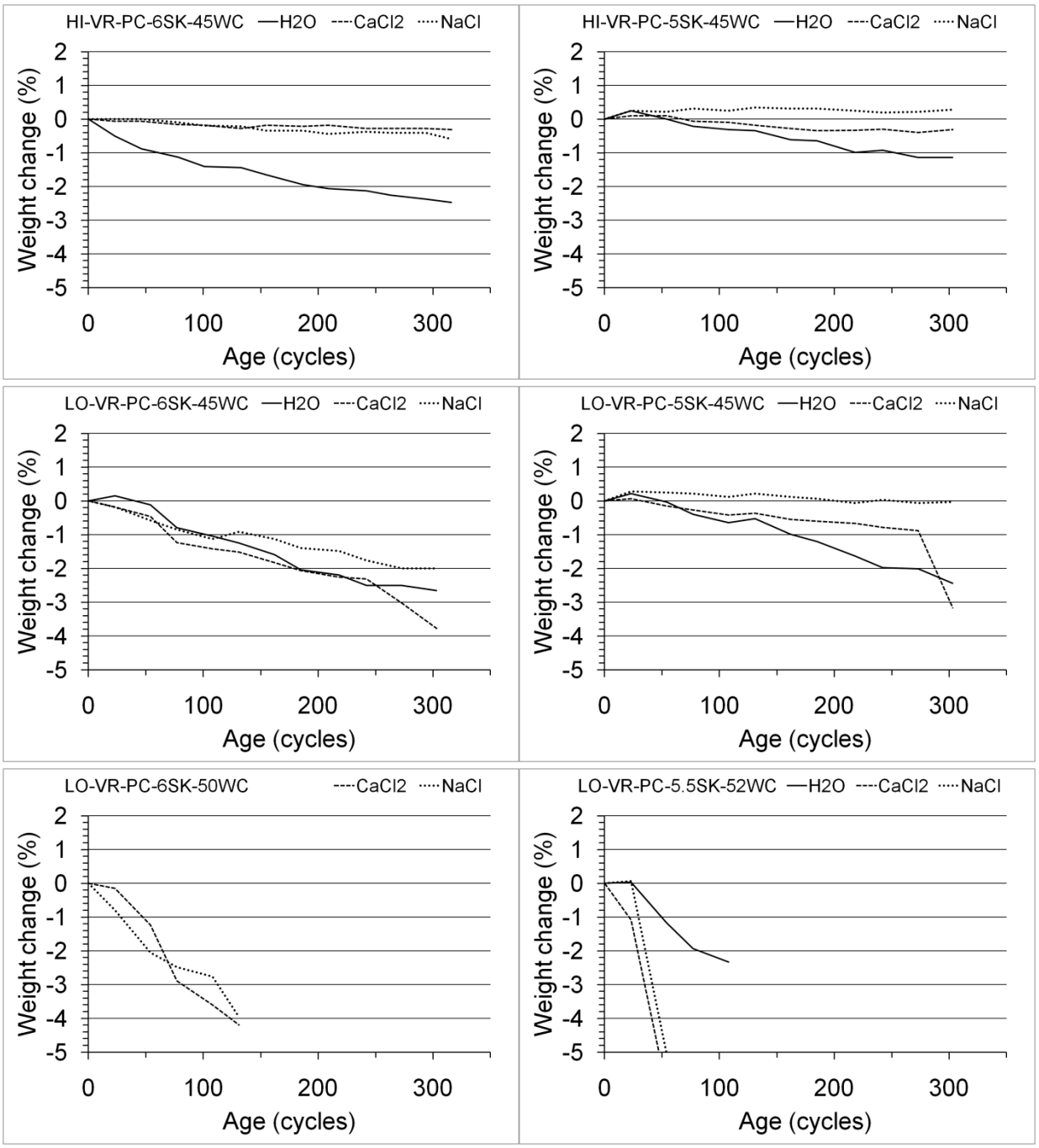

Figure 41: Weight change plots from selected Phase II concrete mixtures exposed to extended F-T cycling test results under different ASTM C66 Procedure A freezing regimes: freeze in water, freeze in 4.0 wt % $CaCl_2$ brine, and freeze in 4.2 wt. % NaCl brine.

5.2.3 Air-Void System Parameters

A flatbed scanner was used to collect images from polished cross-sections through hardened concrete from each mixture, and the images automatically analyzed to compute air-void parameters according to the equations listed in ASTM C457 Standard Test Method for Microscopical Determination of Parameters of the Air-Void System in Hardened Concrete. Details of the flatbed scanner methodology are included in Peterson et al. [2009]. The results of flatbed scanner air-void measurements were included in Tables 4-6 for comparison with the other fresh concrete air tests (i.e. pressure meter, volumetric meter, gravimetric meter, and AVA).

In the flatbed scanner method, a polished slab of concrete is painted black, white powder is pressed into the voids, and an 8-bit grayscale image of the prepared surface is recorded by the flatbed scanner. Bright pixels in the image are classified as air, and relevant statistics (e.g. air content and void frequency) are automatically measured. However, the distinction between pixels bright enough to be counted as air or dark enough to be excluded can be difficult to make. To assist with this process, 20 polished slabs were randomly selected from the 160 polished slabs prepared from the Phase II mixtures, and analyzed by a human operator according to the ASTM C457 Procedure B Modified Point-Count Method. These are referred to as "calibration samples" as they are used to calibrate the software used to discriminate air voids in the images. The same 20 calibration samples were also scanned, and the images subjected to an iterative procedure that compared automatically determined air-void parameters to the manually determined air-void parameters as the grey level threshold used to discriminate between white (i.e. air voids) and black (i.e. cement paste or aggregate) was stepped between the 256 discrete gray levels between pure bright and pure dark. Figure 42 tracks the average difference between the flatbed scanner derived parameters and the manually derived parameters for the 20 calibration samples as the threshold was varied. As shown in Figure 42, the difference achieves a minimum at a threshold level of 174 for the air content, and a minimum at a threshold level of 117 for the void frequency. The mid-point between these two minima was recorded for each of the 20 calibration samples, and the average mid-point value was computed at a threshold of 151. This value was in turn used as the fixed threshold level for the subsequent analysis of the entire population of 160 samples. Figure 43 shows a histogram of optimum threshold levels for the 20 calibration samples. Figure 44 compares the manually determined air-void parameters from the 20 calibration samples to the flatbed scanner determined air-void parameters at the fixed threshold level of 151.

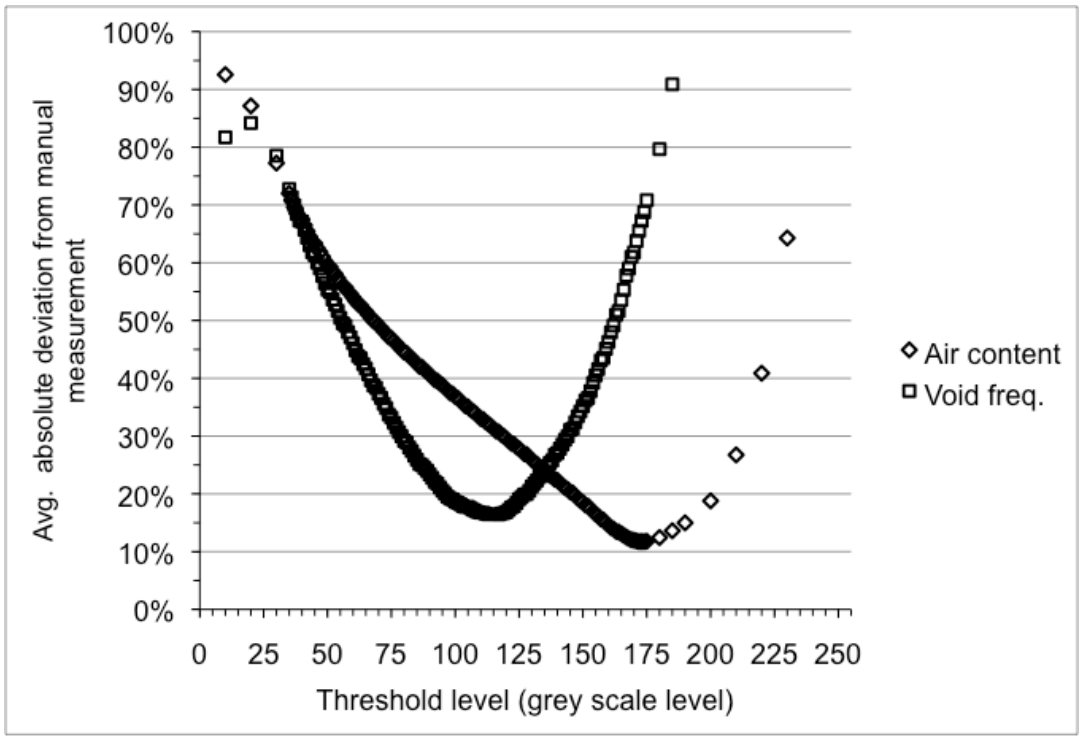

Figure 42: Average absolute deviation between flatbed scanner and manual ASTM 457 measurements of air content and void frequency versus threshold for the 20 calibration samples.

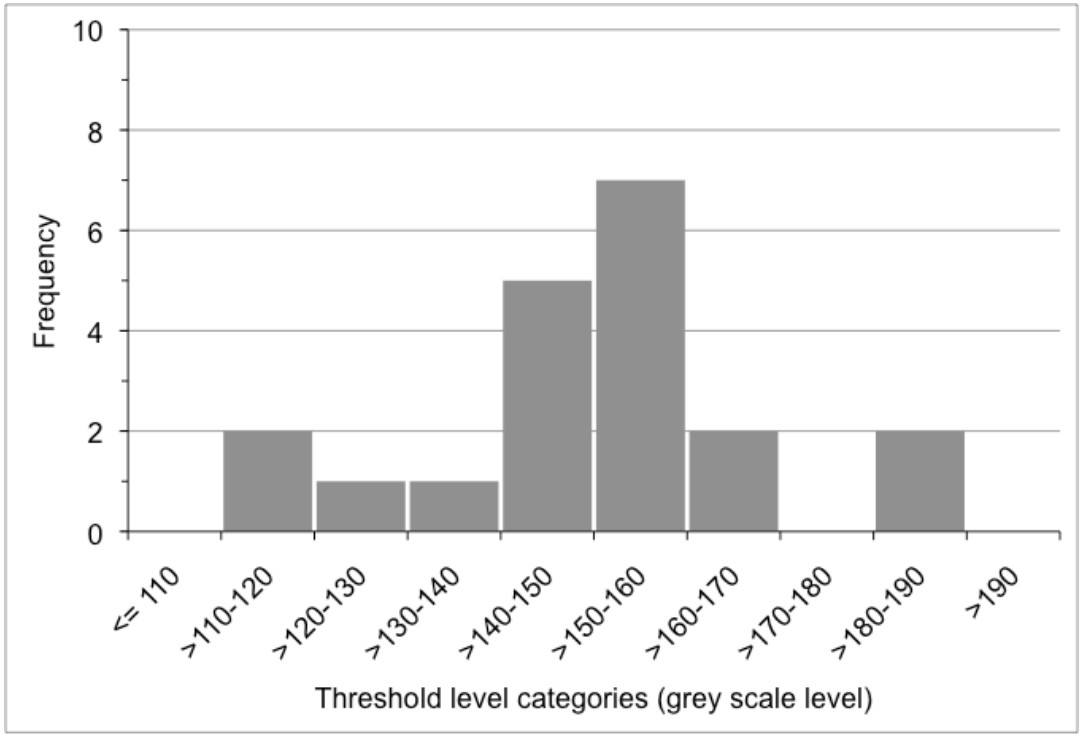

Figure 43: Histogram of optimum threshold levels determined for the 20 training samples.

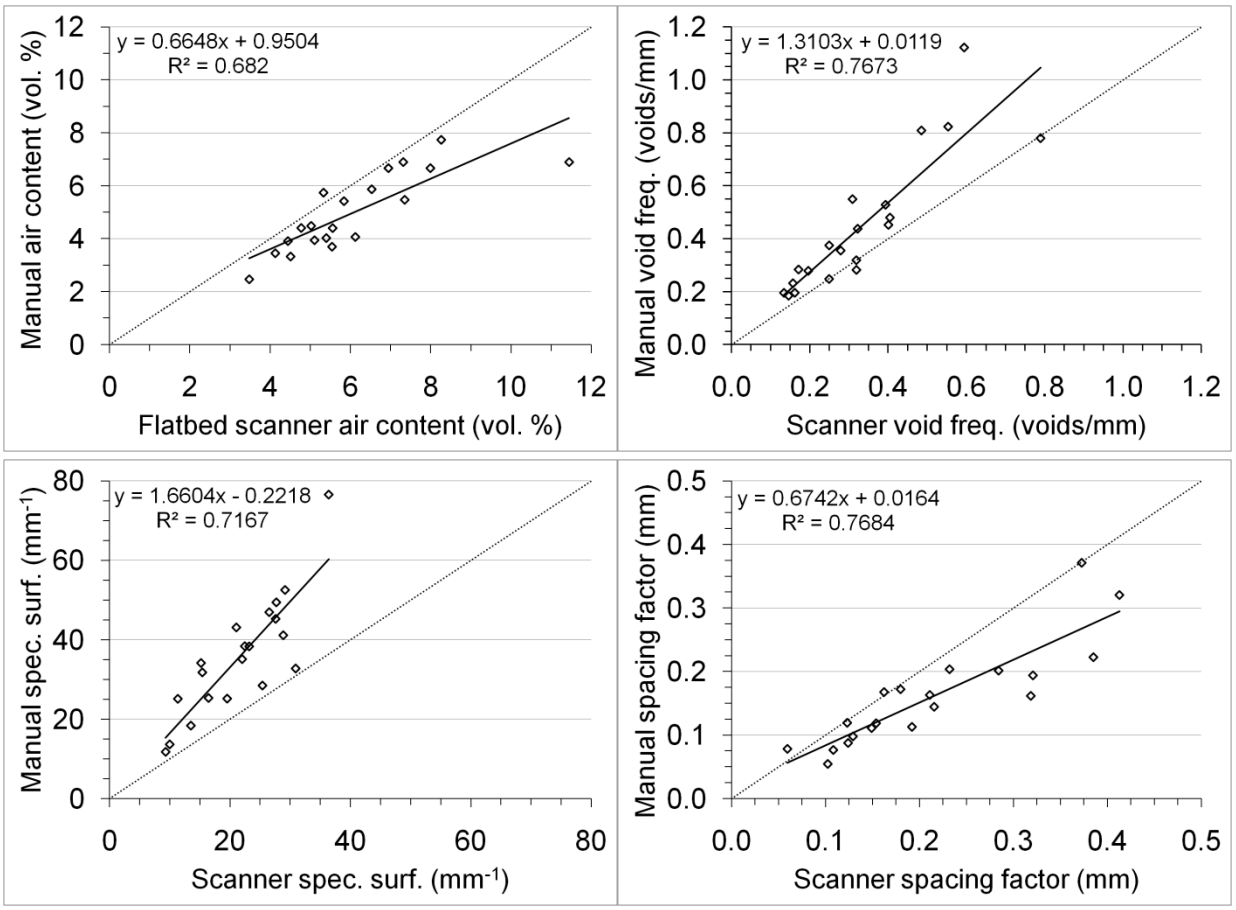

Figure 44: Comparison of air-void parameters measured from manual ASTM C457 and flatbed scanner at a threshold of 151.

5.2.4 Petrographic Examination for Determination of Equivalent w/cm

Tests were performed to estimate the equivalent *w/cm* for selected mixtures using epifluorescence optical microscopy. The technique requires impregnating the concrete thin section specimens with an epoxy containing a fluorescent dye and observing those specimens using an optical microscope equipped to detect the fluorescence from the illuminated specimen rather than the incident light. The intensity of the fluorescence is proportional to the *w/cm* of the hardened cement paste. To estimate the "true" *w/cm* for the specimen, standards must be prepared using the exact same materials used to produce the concrete. In this case, a set of generic standards were used that did not have exactly the same materials and therefore, the estimated *w/cm* is termed the "equivalent" *w/cm*. Generally speaking, the equivalent *w/cm* is very near the true *w/cm* and is therefore commonly used except where very precise estimations of *w/cm* are required.

Fluorescent epoxy impregnated thin sections were prepared from several Phase II low air content (3 vol. % air) concrete mixtures after curing in a saturated limewater bath for approximately 120 days, as listed below.

- LO-VR-PC-6SK-45WC
- LO-VR-PC-6SK-50WC
- LO-VR-PC-5.5SK-52WC
- LO-SYN-PC-6SK-45WC
- LO-SYN-PC-6SK-50WC
- LO-SYN-PC-5.5SK-52WC

Paste fluorescence measurements from the concrete mixtures were compared to measurements from standard air-entrained portland cement 20-30 Ottawa sand mortars made at 0.40, 0.50, and 0.60 *w*/*cm* that had been cured in limewater for 28 days. Prior to thin sectioning, all samples were dried in a 50 °C oven and impregnated with EPO-TEK 301 epoxy in which the resin component had been dosed 1.0 % by weight with DayGlo Tigris Yellow D-043 fluorescent dye. The images were collected in epifluorescent mode with an Olympus BX-60 System Microscope equipped with an Optronics DEI-750 CCD video camera. The G-band was extracted from each 640 x 480 pixel, 2.540 x 1.905 mm, 24-bit RGB image, and the fine aggregate and air-voids manually masked to isolate fluorescence due to the uptake of epoxy into the capillary pores of the hardened cement paste.

Figures 45-47 show the images collected from the mortar standards. Tables 14-16 list the average intensity values for each individual image, and correlated *w*/*cm* values for each individual image based on the linear best fit to the data as shown in the calibration curve of Figure 48. The calibration curve from the mortar standards was applied to the fluorescence measurements from the selected Phase II concrete mixtures. Figures 49-51 show the images collected from the vinsol resin AEA concrete mixtures, and Tables 17-19 list the average intensity values and correlated *w*/*cm* values for each individual image. Figures 52-54 show the images collected from the synthetic AEA concrete mixtures, and Tables 20-22 list the average intensity values and correlated *w*/*cm* values for each individual image. An outline describing the application of epifluorescent methods to *w*/*cm* determination is provided by Jensen et al., (1995).